The first observation of azo-hydrazone and *cis–trans* tautomerisms for disperse yellow dyes and their nickel(II) and copper(II) complexes†

Wei You, Hao-Yu Zhu, Wei Huang,* Bin Hu, Ying Fan and Xiao-Zeng You

Received 10th March 2010, Accepted 7th July 2010
First published as an Advance Article on the web 3rd August 2010
DOI: 10.1039/c0dt00101e

Azo-hydrazone and *cis–trans* tautomerisms have been firstly observed between two disperse yellow dyes (*cis*/*trans*-HL_1 and *cis*-HL_2) and three neutral dye-metal complexes (one mononuclear Ni^{II} complex 3 and two Cu^{II} coordination polymers 4 and 5 formulated as $[Ni(trans\text{-}L_1)_2(CH_3OH)_2]\cdot 2H_2O$, $[Cu(cis\text{-}L_1)_2]_n$ and $[Cu(L_3)(H_2O)]_n$).

Azo dyes and their metal complex dyes are key chromophores in dye chemistry and have found widespread applications in textile, leather and food industries and elsewhere.[1–3] In some cases, azo dyes are also referred to as hydrozone dyes since they can be either in the azo or in the tautomeric form.[4] They are the most widely used class of dyes because of their variable applications in various fields like the dyeing of textile fibers, the coloring of different materials such as wood, wool, yarn, leather, nylon, cotton, metal foil and plastic, the biological and medical investigations, and even the organic synthesis.[5] Moreover, they can be advanced into the materials for non-linear optics and storage of optical information in laser disks.[6] The subtle change of functional groups, the different tautomeric forms and crystallographic arrangements help decide their properties.[7]

Tautomerism, as one of the geometrical isomerisms, is not only important to the dyestuff manufacturers but also to other areas of chemistry. Tautomers in distinctive isomeric forms not only have different colors, but also have different tinctorial strengths (and hence economics) and properties such as color fastness to washing, weathering, rubbing, light, sublimation and perspiration.[8] Single-crystal X-ray diffraction determination is proved to be the most powerful tool to characterize various geometrical isomerisms by its measured bond lengths and angles, dihedral and torsion angles, *etc.*

The dyes having 1-alkyl-5-cyano-2-hydroxy-4-methyl-6-pyridone coupling components have good coloration properties and give bright greenish-yellow hues.[9] In general, they have two enantiotropic isomers, *i.e.* the 2-hydroxy-6-pyridone (azo) form and the pyridine-2,6-dione (hydrazone) form. To date there have been only five structural reports on this family of organic dyes having the above-mentioned *N*-alkyl-pyridone coupling backbones,[10–14] including our contributions of C. I. Disperse Yellow 126, 114, 119 and 211. However, neither azo-hydrazone and *cis–trans* tautomerisms nor dye-metal complexes are mentioned in these documents up until now, which are believed to be very interesting and important issues for the theories and applications of dye chemistry. We report herein the structural and conformational characterizations and computational calculations for two pyridone-based disperse yellow dyes (*cis*/*trans*-HL_1 and *cis*-HL_2‡) as well as a mononuclear nickel(II) complex $[Ni(trans\text{-}L_1)_2(CH_3OH)_2]\cdot 2H_2O$ (**3**) and a cyano-extended one-dimensional (1D) double-ribbon copper(II) coordination polymer $[Cu(cis\text{-}L_1)_2]_n$ (**4**). Furthermore, a cyano-extended 1D layer copper(II) coordination polymer $[Cu(L_3)(H_2O)]_n$ (**5**) is included, which is obtained from the *in situ* Cu^{II} ion catalysis and complexation with the H_2O_2 oxidant of HL_1. In neutral complexes **3**–**5**, ligand L_1 acts as a bidentate chelating ligand in **3** and a tridentate bridging ligand in **4**, while ligand L_3 serves as a tetradentate bridging ligand in **5**.

In this communication, we define the alkyl group (ethyl in HL_1 or methyl in HL_2) bonded to the pyridine nitrogen atom and the *m*-position chlorine atom on the same side of the azo unit as the *cis* configuration, and those on the opposite sides as the *trans* one (Scheme 1). Both *cis*/*trans*-HL_1 and *cis*-HL_2 are the main active ingredients of C. I. disperse yellow 241 dyes and they could be prepared from the pyridine-1-alkyl-3-cyano-4-methyl(ethyl)-2,6-dione coupling components.[9] Like the previously reported six structures with the same backbone but different coupling components, X-ray single-crystal diffraction studies on *cis*/*trans*-HL_1 and *cis*-HL_2 reveal that they are both in the hydrazone form, which could be the general characteristic for this family of disperse yellow dyes. Moreover, ^1H NMR spectra of *cis*/*trans*-HL_1 and *cis*-HL_2 in the $CDCl_3$ solvent exhibit a single peak at 14.97 and 14.93 ppm, respectively, indicative of the existence of a hydrazone proton.

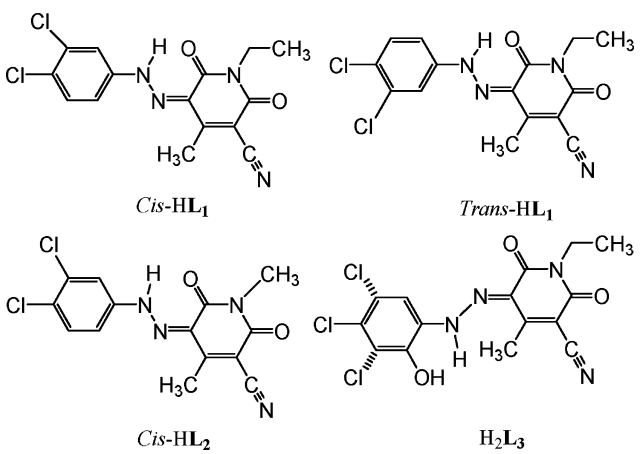

Scheme 1 Solid-state structures for different isomers for HL_1, HL_2 and H_2L_3 in the same pyridine-2,6-dione form.

State Key Laboratory of Coordination Chemistry, Nanjing National Laboratory of Microstructures, School of Chemistry and Chemical Engineering, Nanjing University, Nanjing, 210093, P.R. China. E-mail: whuang@nju.edu.cn; Fax: 86 25 8331 4502; Tel: 86 25 8368 6526

† Electronic supplementary information (ESI) available: DFT calculations, tables for selected bond lengths and angles, hydrogen bonding and π–π stacking interactions in five dye compounds, PXRD and TG-DTA graphs. CCDC reference numbers 760909–760913. For ESI and crystallographic data in CIF or other electronic format see DOI: 10.1039/c0dt00101e

For some azo dyes having aromatic coupling components, it is possible to add one hydroxyl group to the aromatic units directed by the electronic effects of their substituted group(s) in the presence of excess H_2O_2, where the Cu^{II} ion is preferentially selected as a catalyst or a template to form oxidized dye-metal complexes.[15] In this work, **5** has been successfully produced by this strategy and the Cu^{II} ion serves as a catalyst and a metal center for complexation simultaneously (Scheme 2). Compared with the original ligand $\mathbf{L_1}$, a new ligand $\mathbf{L_3}$ is *in situ* formed having an additional phenolic group and it coordinates with the central Cu^{II} ion as a tetradentate bridging ligand.

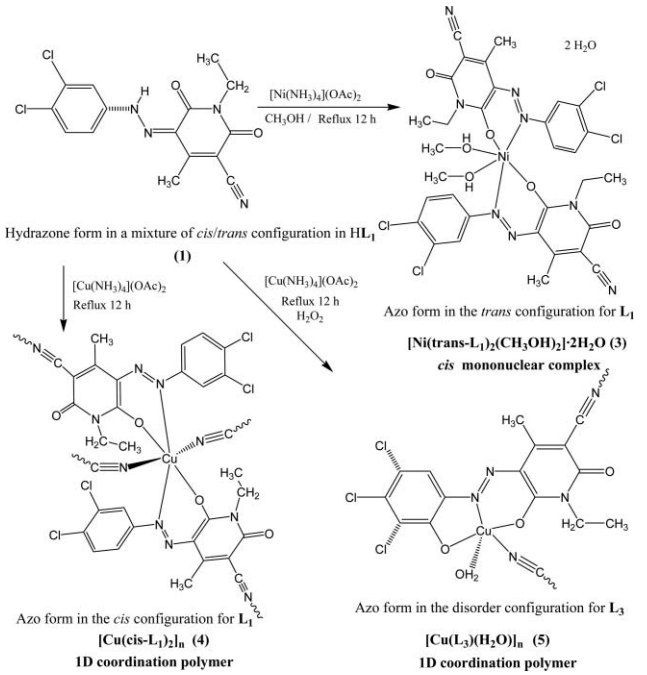

Scheme 2 Schematic illustration for the preparation of dye-metal complexes **3**–**5**.

The FT-IR spectra of *cis*/*trans*-$\mathbf{HL_1}$, *cis*-$\mathbf{HL_2}$ and **3** have single peaks at 2229, 2225 and 2225 cm^{-1}, indicative of the typical absorptions of free CN group. After metal-ion complexation, the absorptions of the CN group shift to a lower wave number of 2212 and 2213 cm^{-1} in **4** and **5**. In the UV/Vis spectra, *cis*/*trans*-$\mathbf{HL_1}$ and *cis*-$\mathbf{HL_2}$ show very analogous intramolecular π–π* transitions centered at 429 and 425 nm because of their structural similarities (Fig. S1, ESI†). After coordination with the Ni^{II} and Cu^{II} ions, the π–π* transitions of $\mathbf{L_1}$ are slightly hypsochromically shifted by 8 and 17 nm in **3** and **4**. Compared with *cis*/*trans*-$\mathbf{HL_1}$, a bathochromic shift of 64 nm is observed in **5** arising from the presence of a more delocalized π-system of $\mathbf{L_3}$ with an additional phenolic group.

X-Ray structural analyses on *cis*/*trans*-$\mathbf{HL_1}$ and *cis*-$\mathbf{HL_2}$§ reveal the existence of two crystallographically independent molecules in the asymmetric unit of $\mathbf{HL_1}$ with equal amount of *cis*-$\mathbf{HL_1}$ and *trans*-$\mathbf{HL_1}$ isomers (Fig. 1). In contrast, there is only one molecule in the asymmetric unit of $\mathbf{HL_2}$ (Fig. S2, ESI†). The difference in their crystallography is suggested to originate from the less steric crowding effect of methyl group in *cis*-$\mathbf{HL_2}$. On considering that the subtle change of substituted groups of the

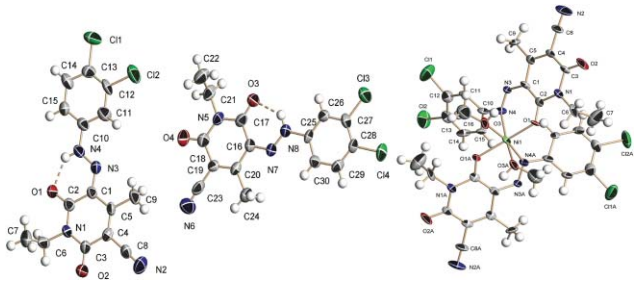

Fig. 1 ORTEP diagrams of *cis*/*trans*-$\mathbf{HL_1}$ (left) and **3** (right) in 30% thermal probability ellipsoids showing hydrazone-azo tautomerisms after metal-ion complexation. Solvent water molecules are omitted for clarity.

dye backbone (ethyl group in $\mathbf{HL_1}$ *versus* methyl group in $\mathbf{HL_2}$) can result in the *cis*/*trans* conformational alteration and possible azo-hydrazone tautomerism, we have carried out density function theory (DFT) computations for single-crystal and the energy-minimized structures of different isomers of *cis*/*trans*-$\mathbf{HL_1}$ and *cis*-$\mathbf{HL_2}$ molecules (see Table S1 for details, ESI†). The results indicate that the hydrazone isomers are more thermally stable than the corresponding azo isomers with the energy gaps of about 150 KJ/mol, and the *trans* isomers are also somewhat more thermally stable than the *cis* ones for both $\mathbf{HL_1}$ and $\mathbf{HL_2}$ with the energy gaps of several to tens of KJ/mol. However, two pairs of isomers are accessible because the calculated energy gaps fall within the range of typical interactions in supramolecular level (several to tens of KJ/mol). The larger energy gaps between the single-crystal structures and the energy-minimized structures in the same hydrazone form for the *cis* and *trans* isomers of $\mathbf{HL_1}$ and the *cis* isomer of $\mathbf{HL_2}$ may be the reflection of the energy compensation of the formation of multiple hydrogen bonding and π–π stacking interactions between neighboring molecules.

Both *cis*/*trans*-$\mathbf{HL_1}$ and *cis*-$\mathbf{HL_2}$ disperse yellow dyes exist in the hydrazone form, which can be deduced by related N–N, C–N, C–C and C–O bond lengths (Table S2, ESI†). Furthermore, the hydrazone H atoms are involved in the intramolecular hydrogen bonds with the 2-position O atoms of pyridyl groups forming six-membered rings (Table S3, ESI†). Actually, higher R_1 and wR_2 values will be generated if the hydrazone hydrogen atoms are added to atoms O1 and O3 in *cis*/*trans*-$\mathbf{HL_1}$ and *cis*-$\mathbf{HL_2}$ to form hydroxyl groups. All the non-hydrogen atoms in *cis*/*trans*-$\mathbf{HL_1}$ and *cis*-$\mathbf{HL_2}$ except one carbon atom of the *N*-substituted ethyl group in $\mathbf{HL_1}$ are essentially coplanar forming extended π-systems, where the dihedral angles between the aromatic rings are 1.52, 1.31 and 3.95° in *cis*-$\mathbf{HL_1}$, *trans*-$\mathbf{HL_1}$ and *cis*-$\mathbf{HL_2}$ molecules.

Different packing structures have been observed for *cis*/*trans*-$\mathbf{HL_1}$ and *cis*-$\mathbf{HL_2}$. The former has two sets of isomeric forms packing along two directions with the dihedral angle of 36.29°, and π–π stacking interactions can be found only between adjacent phenyl and pyridyl rings in *cis*-$\mathbf{HL_2}$ isomers *via* a head-to-tail manner with the centroid–centroid separation of 3.682 Å. In contrast, the latter forms a layer packing with the centroid–centroid separation of 3.820 Å between contiguous aromatic rings as shown in Fig. S3, ESI.†

In complex **3**, the Ni^{II} ion exhibits six-coordinate elongated octahedral geometry and the equatorial plane is composed of two N and two O atoms from two $\mathbf{L_1}$ ligands with the Ni–O and

Ni–N bond lengths of 1.975(6) and 2.071(9) Å (Fig. 1). The apical positions are occupied by two O atoms of coordination methanol molecules with longer Ni–O bond distance of 2.116(9) Å. Moreover, the two $\mathbf{L_1}$ ligands and the two coordination methanol molecules around the Ni^{II} center adopt the *cis* configuration. Due to the steric restriction of coordinative bonds, each $\mathbf{L_1}$ ligand could not be planar and the dihedral angle between the phenyl and pyridyl rings in ligand $\mathbf{L_1}$ turns out to be 32.68°.

It is noted that an interconversion between hydrazone and azo tautomers occurs for $\mathbf{L_1}$ after metal-ion complexation. The related N–N (N3–N4 and N7–N8) and C–C (C1–C2 and C16–C17) bond lengths have been shortened from 1.318(5), 1.298(5) Å and 1.470(7), 1.438(7) Å in $\mathbf{HL_1}$ to 1.276(12) and 1.412(15) Å in **3**, exhibiting more double-bond character. In contrast, their neighboring C–N (C2–N1, C17–N5 and C1–N3, C16–N7) bond lengths have been lengthened from 1.381(6), 1.392(6) Å and 1.316(6), 1.340(6) Å in $\mathbf{HL_1}$ to 1.408(13) and 1.373(14) Å in **3**, displaying predominantly single-bond character. Furthermore, *cis–trans* tautomerism takes place after metal-ion complexation since all the $\mathbf{L_1}$ ligands adopt the *trans* configuration in **3**.

In complex **4**, the Cu^{II} ion adopts a six-coordinate Jahn–Teller elongated octahedral configuration and $\mathbf{L_1}$ adopts the *cis* configuration with respect to the molecular plane (Fig. 2). The basal coordination plane consists of two N and two O atoms from two $\mathbf{L_1}$ ligands with the Cu–O and Cu–N bond lengths of 1.956(5) and 1.975(6) Å, but the apical positions are occupied by two cyanide N atoms from another two $\mathbf{L_1}$ ligands with much longer Cu–N bond lengths of 2.519(7) Å. Different from **3**, each $\mathbf{L_1}$ in **4** serves as a tridentate bridging ligand and a pair of $\mathbf{L_1}$ ligands link adjacent Cu^{II} centers in a reverse fashion. As a result, a cyano-extended 1D double-ribbon Cu^{II} coordination polymer is constituted with the Cu···Cu separation of 9.449 Å (Fig. 3). Because of the fixation of coordination bond, each $\mathbf{L_1}$ in **4** could not maintain the planar structure any more and the dihedral angle between the phenyl and the pyridyl rings is as large as 50.54°. π–π Stacking interactions can be found between every pyridyl pair in the double-ribbon unit with the centroid–centroid contact of 3.876 Å (Fig. 3).

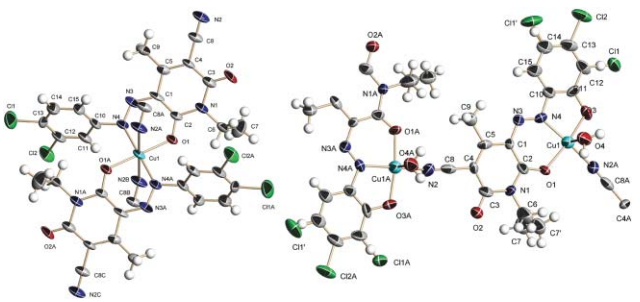

Fig. 2 ORTEP diagrams of molecular structures of **4** (left) and **5** (right) in 30% thermal probability ellipsoids.

The coordination geometry for Cu^{II} center in complex **5** is five-coordinate pyramidal. In this case, ligand $\mathbf{L_3}$ is produced from the *in situ* Cu^{II} catalysis and oxidation of $\mathbf{HL_1}$, where a new coordination site of phenolic O atom is generated. One azo N and two O atoms of $\mathbf{L_3}$ chelate the Cu^{II} center and one cyanide

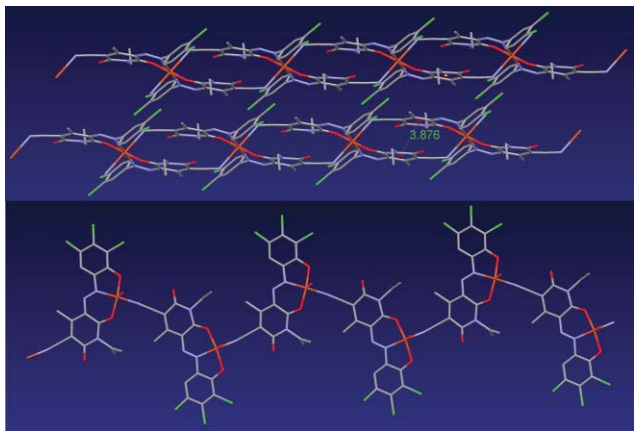

Fig. 3 Perspective views of the different cyano-extended 1D Cu^{II} coordination polymers of **4** (top) and **5** (bottom).

N atom from another $\mathbf{L_3}$ ligand acts as the fourth site of the coordination plane being the Cu–O and Cu–N bond lengths of 1.919(6)–1.961(7) Å. The apical position is occupied by a water molecule with longer Cu–O bond length of 2.273(5) Å. All the non-hydrogen atoms except one ethyl C atom and the apically coordinated water molecule are essentially coplanar in **5**. Compared with *cis*/*trans*-$\mathbf{HL_1}$, $\mathbf{L_3}$ exhibits similar azo-hydrazone tautomerism after metal-ion complexation and it serves as a tetradentate bridging ligand linking contiguous Cu^{II} ions into a cyano-extended 1D layer coordination polymer with the Cu···Cu separation of 9.910 Å (Fig. 3). A dimeric 1D layer is formed where every aqua ligand points to the inner direction and hydrogen bonds are observed between the H atoms of coordination water molecules and their neighboring N, O and Cl atoms. Additionally, π–π stacking interactions are observed between and within different dimeric units with the centroid-centroid separations of 3.731 and 3.788 Å (Fig. S4, ESI†).

The pure phase of compounds *cis*/*trans*-$\mathbf{HL_1}$, *cis*-$\mathbf{HL_2}$ and **3**–**5** is confirmed by powder X-ray diffraction (PXRD) patterns (Fig. S5–9, ESI†). TG-DTA analyses for *cis*/*trans*-$\mathbf{HL_1}$ and *cis*-$\mathbf{HL_2}$ reveal that the former starts to decompose from 242 °C with a DTA peak at 285 °C, while the latter starts to decompose from 225 °C with a DTA peak at 243 °C (Fig. S10 and S11, ESI†). This is because of the presence of less van der Waals force between molecules in *cis*-$\mathbf{HL_2}$. In comparison, the thermal stabilities of neutral dye-metal complexes **3**–**5** have been greatly improved (Fig. S12–14, ESI†). Complex **3** starts to lose two coordination methanol molecules at 102 °C with a DTA peak at 110 °C, and then it decomposes from 278 °C and three continuous weight loss processes take place with DTA peaks at 362, 396 and 412 °C, respectively. In contrast, **4** shows a continuous weight loss process from 331 °C, which is higher than that in **3**, and the DTA peak corresponding to this stage centered at 344 °C. Thermal analysis for **5** reveals two DTA peaks centered at 169 and 463 °C, indicative of the loss of coordination water molecules and the decomposition process of the compound, respectively.

In summary, two pyridone-based disperse yellow dyes in the hydrazone form having different ethyl and methyl substituents have been structurally characterized and compared. After metal-ion complexation with Ni^{II} and Cu^{II} ions, conformational

interconversions between azo/hydrazone and *cis*/*trans* isomers have been achieved, where the azo ligands show bidentate, tridentate and tetradentate coordination modes. In addition, the H_2O_2 oxidation of HL_1, catalyzed and *in situ* coordinated by Cu^{II} ion, has been explored. To our knowledge, this is the first study on the coordination chemistry of pyridyl dione involved dyes and also the first observation of azo-hydrazone and *cis*–*trans* tautomerisms before and after metal-ion complexation.

Acknowledgements

W. H. would like to acknowledge the Major State Basic Research Development Programs (Nos. 2007CB925101, 2006CB806104 and 2011CB933300), the National Natural Science Foundation of China (Nos. 20871065 and 20721002) and the Jiangsu Province Department of Science and Technology (No. BK2009226) for financial aid.

Notes and references

‡ Preparation of *cis*/*trans*-HL_1 and *cis*-HL_2: The two disperse yellow dyes were prepared by the coupling reactions from pyridine-1-alkyl-3-cyano-4-methyl-2,6-dione (L_1, alkyl = ethyl; L_2, alkyl = methyl) and according to a literature method.[10] Single crystals of *cis*/*trans*-HL_1 and *cis*-HL_2 suitable for X-ray structural analysis were obtained from methanol *via* slow evaporation in air at room temperature. *Cis*/*trans*-HL_1: Anal. Calcd. for $C_{15}H_{12}Cl_2N_4O_2$: C, 51.30; H, 3.44; N, 15.95%. Found: C, 51.22; H, 3.61; N, 15.85%. Main FT-IR absorptions (KBr pellets, ν, cm^{-1}): 3423 (vs), 2979 (w), 2927 (w), 2228 (w), 1677 (m), 1639 (s), 1516 (s), 1422 (m), 1398 (m), 1379 (m), 1267 (s), 1186 (m), 1120 (m), 1092 (m), and 1036 (m). ^{1}H NMR (500 MHz, $CDCl_3$) δ = 14.97 (s, 1H, NH), 7.62 (d, 1H, ArH), 7.50 (d, 1H, ArH), 7.32 (d, 1H, ArH), 4.06 (q, 2H, CH_2), 2.64 (s, 3H, Me), 1.26 (t, 3H, Me). UV/Vis in methanol: λ_{max} = 429 nm. *Cis*-HL_2: Anal. Calcd. for $C_{14}H_{10}Cl_2N_4O_2$: C, 49.87; H, 2.99; N, 16.62%. Found: C, 49.72; H, 3.01; N, 16.53%. Main FT-IR absorptions (KBr pellets, ν, cm^{-1}): 3416 (vs), 2925 (w), 2225 (w), 1678 (m), 1636 (s), 1514 (s), 1395 (m), 1266 (m), 1178 (m), 1120 (m), 1084 (m), and 1038 (m). ^{1}H NMR (500 MHz, $CDCl_3$) δ = 14.93 (s, 1H, NH), 7.62 (d, 1H, ArH), 7.55 (d, 1H, ArH), 7.34 (d, 1H, ArH), 3.39 (s, 3H, Me), 2.65 (s, 3H, Me). UV/Vis in methanol: λ_{max} = 425 nm. Preparation of [Ni(*trans*-L_1)$_2$(CH_3OH)$_2$]·2H_2O (**3**): A methanol solution (10 cm^3) of Ni(CH_3COO)$_2$·4H_2O (0.020 g, 0.08 mmol) was added into a methanol solution (20 cm^3) of HL_1 (0.056 g, 0.16 mmol). The mixture was slowly heated to 50 °C and a 0.5 cm^3 of concentrated ammonia was added, and then the mixture was refluxed for 12 h. The filtered solution was cooled to room temperature, and dark brown single crystals of **3** suitable for X-ray structural analysis were collected *via* 7 d slow evaporation in air. Yield: 0.056 g (81.5%) based on metal. Anal. Calcd. for $NiC_{32}H_{34}Cl_4N_8O_8$: C, 44.74; H, 3.99; N, 13.04%. Found: C, 44.80; H, 4.03; N, 12.97%. Main FT-IR absorptions (KBr pellets, ν, cm^{-1}): 3417 (b, s), 2980 (w), 2928 (w), 2221 (w), 1674 (m), 1640 (s), 1557 (s), 1514 (w), 1395 (m), 1367 (s), 1267 (m), 1089 (s), and 627 (m). UV/Vis in methanol: λ_{max} = 421 nm. Preparation of [Cu(*cis*-L_1)$_2$]$_n$ (**4**): A methanol solution (10 cm^3) of Cu(CH_3COO)$_2$·H_2O (0.016 g, 0.08 mmol) was added into a methanol solution (20 cm^3) of HL_1 (0.056 g, 0.16 mmol) and NaOMe (0.100 g). The mixture was stirred and refluxed for 12 h. The filtered solution was cooled to room temperature, and dark red single crystals of **4** suitable for X-ray structural analysis were collected *via* 3 d slow evaporation in air. Yield: 0.048 g (78.5%) based on metal. Anal. Calcd. for $CuC_{30}H_{22}Cl_4N_8O_4$: C, 47.17; H, 2.90; N, 14.67%. Found: C, 47.20; H, 2.96; N, 14.62%. Main FT-IR absorptions (KBr pellets, ν, cm^{-1}): 3442 (b, s), 2980 (w), 2928 (w), 2212 (w), 1674 (m), 1640 (s), 1594 (s), 1525 (m), 1395 (m), 1382 (s), 1265 (m), 1089 (s), and 627 (m). UV/Vis in methanol: λ_{max} = 412 nm. Preparation of [Cu(L_3)(H_2O)]$_n$ (**5**): A DMF solution (30 cm^3) of Cu(CH_3COO)$_2$·H_2O (0.048 g, 0.24 mmol) and HL_1 (0.112 g, 0.24 mmol) was cooled to 0 °C with external cooling, and 3 cm^3 of 30% hydrogen peroxide was added dropwise in order that the temperature of mixture did not exceed 5 °C. The color of solution turned out to be vermillion after several minutes, and it was stirred at 0–5 °C for 3 h. The mixture was filtered and the filtrate was condensed to 5 cm^3 by a rotatory evaporator. Ethyl acetate (30 cm^3) was added into the residue to precipitate **5**, and the solid was filtered, washed by ethyl acetate and dried *in vacuo*. Yield: 0.085 g (79.3%) based on metal. Red single crystals of **5** suitable for X-ray structural analysis were obtained from a mixture of DMF and methanol in a ratio of 1 : 3 (v/v) *via* 15 d slow evaporation in air. Anal. Calcd. for $CuC_{15}H_{12}Cl_2N_4O_4$: C, 40.33; H, 2.70; N, 12.54%. Found: C, 40.39; H, 2.85; N, 12.44%. Main FT-IR absorptions (KBr pellets, ν, cm^{-1}): 3425 (vs), 2974 (w), 2932 (w), 2213 (w), 1658 (s), 1510 (w), 1440 (m), 1393 (s), 1192 (s), 1102 (m), 1039 (m), and 624 (m). UV/Vis in methanol: λ_{max} = 493 nm.

§ X-Ray crystallographic data for compound *cis*/*trans*-HL_1: $C_{15}H_{12}Cl_2N_4O_2$, M = 351.19, T = 291(2) K, monoclinic, space group, $P2_1/c$, a = 7.369(2) Å, b = 20.067(4) Å, c = 21.444(5) Å, β = 94.617(4)°, V = 3160.5(12) Å^3, Z = 8, μ = 0.425 mm^{-1}, D_c = 1.476 g cm^{-3}, F(000) = 1440, reflections collected/independent 15 882/5571, refinement method, full-matrix least-squares on F^2, parameters, 419, S = 0.667, R_1 [$I > 2\sigma(I)$] = 0.0549, wR_2 (all data) = 0.1069. Residual electron density, 0.44/–0.32 e Å^{-3}. X-Ray crystallographic data for compound *cis*-HL_2: $C_{14}H_{10}Cl_2N_4O_2$, M = 337.16, T = 291(2) K, monoclinic, space group, $P2_1/n$, a = 8.541(1) Å, b = 11.969(2) Å, c = 14.529(2) Å, β = 102.756(2)°, V = 1448.5(3) Å^3, Z = 4, μ = 0.460 mm^{-1}, D_c = 1.546 g cm^{-3}, F(000) = 688, reflections collected/independent 7116/2539, refinement method, full-matrix least-squares on F^2, parameters, 201, S = 0.934, R_1 [$I > 2\sigma(I)$] = 0.0635, wR_2 (all data) = 0.1877. Residual electron density, 0.90/–0.34 e Å^{-3}. X-Ray crystallographic data for nickel(II) complex **3**: $NiC_{32}H_{34}Cl_4N_8O_8$, M = 859.18, T = 291(2) K, orthorhombic, space group, $Ccc2$, a = 21.943(3) Å, b = 24.179(4) Å, c = 7.530(1) Å, β = 90°, V = 3995.0(10) Å^3, Z = 4, μ = 0.810 mm^{-1}, D_c = 1.429 g cm^{-3}, F(000) = 1768, reflections collected/independent 9374/3395, refinement method, full-matrix least-squares on F^2, parameters, 225, S = 1.080, R_1 [$I > 2\sigma(I)$] = 0.0923, wR_2 (all data) = 0.1931. Residual electron density, 0.98/–0.80 e Å^{-3}. X-Ray crystallographic data for copper(II) complex **4**: $CuC_{30}H_{22}Cl_4N_8O_4$, M = 763.91, T = 291(2) K, triclinic, space group, $P\bar{1}$, a = 7.642(7) Å, b = 8.378(8) Å, c = 13.350(12) Å, α = 72.398(15)°, β = 87.327(15)°, γ = 72.126(13)°, V = 774.4(12) Å^3, Z = 1, μ = 1.102 mm^{-1}, D_c = 1.638 g cm^{-3}, F(000) = 387, reflections collected/independent 3838/2661, refinement method, full-matrix least-squares on F^2, parameters, 216, S = 1.003, R_1 [$I > 2\sigma(I)$] = 0.0775, wR_2 (all data) = 0.2541. Residual electron density, 1.08/–1.70 e Å^{-3}. X-Ray crystallographic data for copper(II) complex **5**: $CuC_{15}H_{12}Cl_2N_4O_4$, M = 446.73, T = 291(2) K, monoclinic, space group, $P2_1/n$, a = 10.500(2) Å, b = 14.588(3) Å, c = 11.537(2) Å, β = 102.162(4)°, V = 1727.6(6) Å^3, Z = 4, μ = 1.603 mm^{-1}, D_c = 1.718 g cm^{-3}, F(000) = 900, reflections collected/independent 8669/3039, refinement method, full-matrix least-squares on F^2, parameters, 252, S = 0.771, R_1 [$I > 2\sigma(I)$] = 0.0625, wR_2 (all data) = 0.1184. Residual electron density, 0.39/–0.47 e Å^{-3}.

1 D. R. Waring and G. Halas, *The chemistry and application of dyes* New York: Plenum1990.
2 H. Zollinger, *Color chemistry: synthesis, properties and applications of organic dyes and pigments*, *3rd Ed*, Weinheim, Germany, Wiley-VCH, 2003; R. Rys and H. Zollinger, *Fundamentals of Chemistry and Application of Dyes*, John Wiley and Sons, London, 1972.
3 A. D. Town, *Dyes Pigm.*, 1999, **42**, 3; R. R. Avirah, K. Jyothish and D. Ramaiah, *J. Org. Chem.*, 2008, **73**, 274.
4 G. Pavlovic, L. Racane, H. Cicak and V. T. Kulenovic, *Dyes Pigm.*, 2009, **83**, 354; J. J. Lee, N. K. Han, W. J. Lee, J. H. Choi and J. P. Kim, *Rev. Prog. Color. Relat. Top.*, 2002, **118**, 154.
5 H. S. Bhatti and S. Seshadri, *Rev. Prog. Color. Relat. Top.*, 2004, **120**, 151; J. B. Dickey, E. B. Towne, M. S. Bloom, W. H. Moore, H. M. Hill, H. Heynemann, D. G. Hefberg, D. C. Sievers and M. V. Otis, *J. Org. Chem.*, 1959, **24**, 187.
6 R. J. H. Clark, R. E. Hester, *Advances in materials science spectroscopy* New York Wiley and Sons1991; H. Bach, K. Anderle, T. Fuhrmann, J. H. Wendorff, *J. Phys. Chem.* 1996, 100, 4135K. Taniike, T. Matsumoto, T. Sato, Y. Ozaki, K. Nakashima, K. Iriyama, *J. Phys. Chem.* 1996, 100, 15508.
7 N. Biswas and S. Umapathy, *J. Phys. Chem. A*, 2000, **104**, 2734; I. Willner and S. Rubin, *Angew. Chem., Int. Ed. Engl.*, 1996, **35**, 367; S. Das, C. H. Hung and S. Goswami, *Inorg. Chem.*, 2003, **42**, 8592.
8 Y. Okada, T. Hihara and Z. Morita, *Dyes Pigm.*, 2008, **78**, 179; Y. Okada, T. Hihara and Z. Morita, *Dyes Pigm.*, 2008, **79**, 111; A. S. Özen, V. Aviyente, G. T. Güyer and N. H. Ince, *J. Phys. Chem. A*, 2005, **109**, 3506; A. S. Özen, P. Doruker and V. Aviyente, *J. Phys. Chem. A*, 2007, **111**, 13506.

9 S. Helmut, U. S. Patent, *Disperse Azo Dye Mixtures*, WO2006/072560.
10 H. F. Qian, *Acta Crystallogr., Sect. C: Cryst. Struct. Commun.*, 2006, **62**, o62.
11 W. Huang and H. F. Qian, *Dyes Pigm.*, 2008, **77**, 446.
12 W. Huang, *Dyes Pigm.*, 2008, **79**, 69.
13 S. N. Black, R. J. Davey, A. M. Z. Slawin and D. J. Williams, *Acta Crystallogr., Sect. C: Cryst. Struct. Commun.*, 1992, **48**, 323.
14 J. Prikryl, B. Kratochvil, J. Ondracek, J. Maixner, J. Klicnar and K. Huml, *Collect. Czech. Chem. Commun.*, 1993, **58**, 2121.
15 M. Idelson, I. R. Karadt, B. H. Mark, D. O. Rickter and V. H. Hooper, *Inorg. Chem.*, 1967, **6**, 450.

